RESEARCH ARTICLE

Construction of oxime-functionalized PCN-222 based on the directed molecular structure design for recovering uranium from wastewater

Changlong Bi[1] · Chunhong Zhang[1,2] · Chao Wang[1,2] · Lien Zhu[1] · Ruiqi Zhu[1] · Lijia Liu[1,2] · Yudan Wang[1] · Fuqiu Ma[2,3] · Hongxing Dong[1]

Abstract

The directed construction of productive adsorbents is essential to avoid damaging human health from the harmful radioactive and toxic U(VI)-containing wastewater. Herein, a sort of Zr-based metal organic framework (MOF) called PCN-222 was synthesized and oxime functionalized based on directed molecular structure design to synthesize an efficient adsorbent with antimicrobial activity, named PCN-222-OM, for recovering U(VI) from wastewater. PCN-222-OM unfolded splendid adsorption capacity (403.4 mg·g^{-1}) at pH = 6.0 because of abundant holey structure and mighty chelation for oxime groups with U(VI) ions. PCN-222-OM also exhibited outstanding selectivity and reusability during the adsorption. The XPS spectra authenticated the -NH and oxime groups which revealed a momentous function. Concurrently, PCN-222-OM also possessed good antimicrobial activity, antibiofouling activity, and environmental safety; adequately decreased detrimental repercussions about bacteria and *Halamphora* on adsorption capacity; and met non-toxic and non-hazardous requirements for the application. The splendid antimicrobial activity and antibiofouling activity perhaps arose from the Zr$_6$(μ_3-O)$_4$(μ_3-OH)$_4$(H$_2$O)$_4$(OH)$_4$ clusters and rich functional groups within PCN-222-OM. Originally proposed PCN-222-OM was one potentially propitious material to recover U(VI) in wastewater on account of outstanding adsorption capacity, antimicrobial activity, antibiofouling activity, and environmental safety, meanwhile providing a newfangled conception on the construction of peculiar efficient adsorbent.

Keywords U(VI) adsorption · Wastewater · Metal organic framework · Antimicrobial activity · Oxime functionalization

Introduction

Recently, the energy is very limited, but the demand for it is on the increase (Li et al. 2021a; Wang et al. 2021a). As a low-carbon and great-density energy, nuclear energy is becoming increasingly important, which can fully meet

---

Responsible Editor: Tito Roberto Cadaval Jr

Highlights
1. New adsorbent PCN-222-OM was developed based on directed molecular structure design.
2. PCN-222-OM had good environmental safety and antimicrobial and antibiofouling activity.
3. PCN-222-OM showed outstanding U(VI) adsorption capacity; Q$_e$ reached 403.4 mg·g^{-1}.
4. Adsorption mechanism was the co-effect of coordination and electrostatic interaction.
5. PCN-222-OM possessed great potential to efficiently recover U(VI) from wastewater.

Extended author information available on the last page of the article

the energy demand in the contemporary world and lessen environmental destruction (Willauer et al. 2015). With the booming advancement of nuclear energy, uranium (U(VI)) requirements are also on the rise globally (Yan et al. 2011; Lin et al. 2022). While U(VI) plays a vital role in the nuclear energy, it is baleful to human health and can cause varied environmental problems as a result of strong toxicity and radioactivity (El-Din et al. 2018; Singh et al. 2021). Thereby, the U(VI) recovery in wastewater is great importance to environmental protection, and it is also very essential to seek novel adsorbents to efficiently recover U(VI) in wastewater.

Nowadays, numbers of technologies were employed in recovering U(VI) ions out of wastewater (Khedr 2015; Li et al. 2017a, 2020a; Tolkou et al. 2020; Bi et al. 2021; Liu et al. 2021; Chen et al. 2022; Xue et al. 2022). Among the many existing technologies, the adsorption has been acknowledged as a very efficient means for convenient operation, security, practicability, and ecological protection (Anirudhan and Jalajamony 2013; Arica and

Bayramoglu 2016). Undoubtedly, the key to adsorption method is to exploit new and effectual adsorbents to ameliorate adsorption performance (Bi et al. 2022). U(VI) adsorbents of sorts such as organic polymers, inorganic materials, biological materials, covalent organic frameworks (COFs), and MOFs were utilized in wastewater (Yang et al. 2019; Ma et al. 2020; Li et al. 2020b, 2021b; Liang et al. 2021). Among them, MOFs attracted widespread interest for its glorious framework stability, specific surface area, and regular porousness (Carboni et al. 2013; Wang et al. 2015; Li et al. 2017b). Quite a few scholars have designed and synthesized various MOF-based adsorbents with magnificent U(VI) adsorption performances from wastewater (Li et al. 2018; Zhang et al. 2019a; Wang et al. 2021b). However, many microorganisms in wastewater can exert significant detrimental impacts upon adsorption capacity for MOF-based adsorbents (Park et al. 2016). The reason for the greatly reduced adsorption performance is that microorganisms can be attached to the adsorbent's surface and multiply in its internal pores, thus blocking the pores and covering the active sites of U(VI) adsorption (Mei et al. 2022; Wang et al. 2022). Consequently, it is very necessary to devise an innovative adsorbent with conspicuous adsorption capacity and antimicrobial activity for authentic wastewater treatment.

A Zr-based MOF with the name of PCN-222 was thought to be an optimistical MOF to design enormously efficacious U(VI) adsorbents because of subsequent superiorities (Feng et al. 2012). Firstly, the synthesis procedure of PCN-222 is uncomplicated and its preparation process is non-polluting to the environment (Liu et al. 2020a). Secondly, PCN-222 can be easily modified by the introduction of solvent-assisted ligands (Li et al. 2019). Thirdly, in comparison with other MOFs, PCN-222 has more lasting biggish channels, preferred metal combining competence and acid–base-resisting peculiarities, which can exhibit a good U(VI) adsorption performance in a broad range of pH values (Yang et al. 2021). Fourthly, PCN-222 possessed a certain antimicrobial activity at the presence of $Zr_6(\mu_3\text{-}O)_4(\mu_3\text{-}OH)_4(H_2O)_4(OH)_4$ clusters, reducing the damaging impact of microorganism on U(VI) adsorption performance (Aguado et al. 2014; Zheng et al. 2020). Thus, PCN-222 is a promising MOF with regard to high-efficiency U(VI) adsorbent exploitation from wastewater. Moreover, highly efficient chelating groups are also important as to the construction of efficient U(VI) adsorbents (Bai et al. 2020a; Zeng et al. 2021; Liu et al. 2022). It is well-known that the amidoxime group has excellent U(VI) selectivity and has been widely applied to adsorption, but the synthesis of amidoxime groups required highly poisonous cyanide, incurring significant risks for environment and human health (Paz et al. 2010; Kandre et al. 2013; Rahman et al. 2016). In comparison with amidoxime groups, the oxime-group raw materials are non-toxic and harmless

(Damljanovic et al. 2006). More importantly, the oxime group also has exhibited outstanding selective adsorption performances to U(VI) ions (Tian et al. 2011).

In view of this, a novel adsorbent (PCN-222-OM) with outstanding U(VI) adsorption capacity and antimicrobial activity was synthesized through PCN-222 oxime functionalization founded on the directed molecular structure design to recover U(VI) from wastewater for the environmental protection and pollution control. PCN-222-OM with plenteous oxime groups possessed glorious U(VI) adsorption capacity and selectivity under weak acid condition, which also had high selective U(VI) removal rate, and the residual U(VI) concentration after adsorption could meet discharge standards. The potential adsorption mechanism was considered to be a comprehensive consequence of coordination and electrostatic interaction; the N–H and oxime groups fulfilled a momentous function in adsorption process of PCN-222-OM. Simultaneously, PCN-222-OM also possessed outstanding antimicrobial activities against *E. coli* and *Staphylococcus aureus*, which effectively reduced negative impacts upon the adsorption performances. All in all, PCN-222-OM was an auspicious adsorbent to recover U(VI) from wastewater for the environmental protection and pollution control, which also provides a fresh mind as for the construction of efficient adsorbent.

Experimental

PCN-222-AD and intermediate synthesization

The activated PCN-222 and PCN-222-NH$_2$ were synthesized throughout solvothermal method based on previous literatures (He et al. 2018; Li et al. 2019). The course was documented in supporting documents (Section S3). Thereupon, PCN-222-NH$_2$ (0.05 g) was allocated to mixed toluene solution (35 mL) containing racemic-2,2′-bis(diphenylphosphino)-1,1′-binaphthyl (BINAP) and tris(dibenzylideneacetone)dipalladium (Pd$_2$(dba)$_3$) under N$_2$ condition to acquire an even mixed solution. Whereafter, 5 mL toluene containing 3-bromopropanal (0.3 g) was injected into the mixed solution mentioned above, which was warmed to 100 ℃ and reacted under N$_2$ condition for 48 h. The suspension was under centrifugation and cleansed by toluene, methanol, and deionized water ordinally; PCN-222-AD was attained after resulting deposition dried out at 50 °C.

PCN-222-OM synthesization

Synthesized PCN-222-AD (0.5 g) had been dispersed to methanol/deionized water (1:1, v:v, 30 mL), NH$_2$OH·HCl

(2.0 g), and Na_2CO_3 (0.9 g) continuously added with stirring. After 24 h of refluxing at 70 °C, the suspension was separated and cleansed in methanol and deionized water ordinally. After drying up the clean deposition at 60 °C overnight, PCN-222-OM was achieved.

Batch adsorption and regeneration experiments

The influences of various factors on adsorption performances were investigated, which mainly included pH value, initial U(VI) concentration, adsorbent dosage, contact time, and temperature. Relevant detail was displayed under supporting information file (Section S4). Furthermore, the desorption and regeneration experiments were also done and the procedures are demonstrated in Section S5 of supporting information file.

Adsorption in simulated nuclear industry wastewater

The simulated nuclear industry wastewater samples with different U(VI) concentrations were prepared in accordance with a shop inspection report about nuclear fuel-element-plant wastewater, to evaluate the selective adsorption capacity of PCN-222-OM to U(VI) ions. The specific steps of adsorption experiments in simulated nuclear industry wastewater are displayed in Section S6 of the supporting information file.

Antimicrobial activity experiments

PCN-222-OM as well as intermediate antimicrobial activity about *E. coli* and *S. aureus* were measured in accordance with our group's previous researches (Bi et al. 2023). The related experiments conducted in this study mainly included minimum inhibitory concentration (MIC), inhibition zone test, and inhibition of bacterial growth curve. The specific

steps of antimicrobial activity experiments are displayed in Section S7 of the supporting information file.

Result and discussions

Synthetic process of PCN-222-OM

A schematic diagram about PCN-222-OM synthesis is exhibited in Fig. 1. First of all, $Zr_6(\mu_3-O)_4(\mu_3-OH)_4(H_2O)_4(OH)_4$ clusters within PCN-222 were modified by aminomethylphosphonic acid to obtain PCN-222-NH_2 with abundant amino groups. Secondly, 3-bromopropanal was used as a modifying agent to convert amino groups into aldehyde groups and PCN-222-AD was obtained. Finally, in order to produce oxime groups, PCN-222-AD was ulteriorly converted through the oximation reaction and PCN-222-OM was triumphantly obtained.

Morphology

TEM images and TEM-EDS mappings for PCN-222 and PCN-222-OM are evinced in Fig. 2; PCN-222 had a tubular structure at 2.3 μm length and obvious crystal lattices at more enormous magnification. After oxime modification, PCN-222-OM was much coarser than the initial PCN-222, yet its framework structure, crystal lattice, and dimension essentially stayed unchanged. TEM-EDS mappings demonstrated the well-proportioned distribution for C, N, O, Zr, and P elements inside PCN-222-OM, and the uniformed P element distribution proved PCN-222 oximation modification was possibly successful.

Structures

FT-IR analysis

Figure 3a illustrated the FT-IR spectra about PCN-222-OM and its intermediates; PCN-222 characteristic peaks were
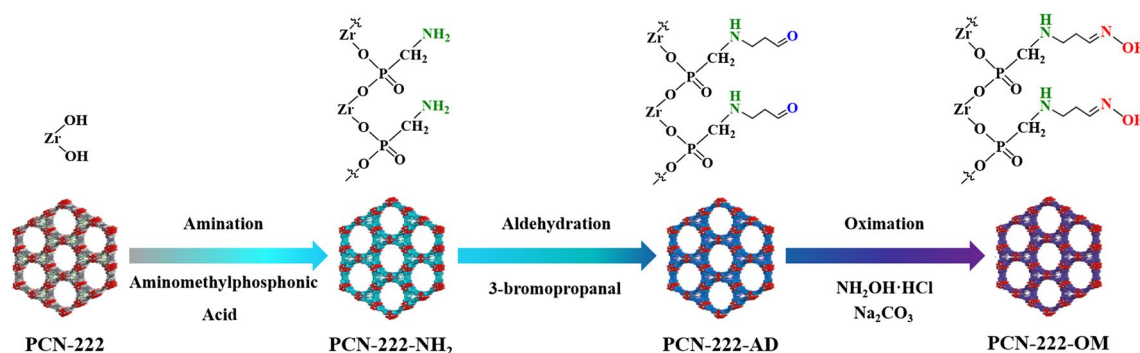

Fig. 1 Schematic diagram of synthetic procedures of PCN-222-OM

Fig. 2 **a** TEM image and TEM-EDS mappings of PCN-222 (O, N, Zr, C). **b** TEM image and TEM-EDS mappings of PCN-222-OM (C, O, N, Zr, P)
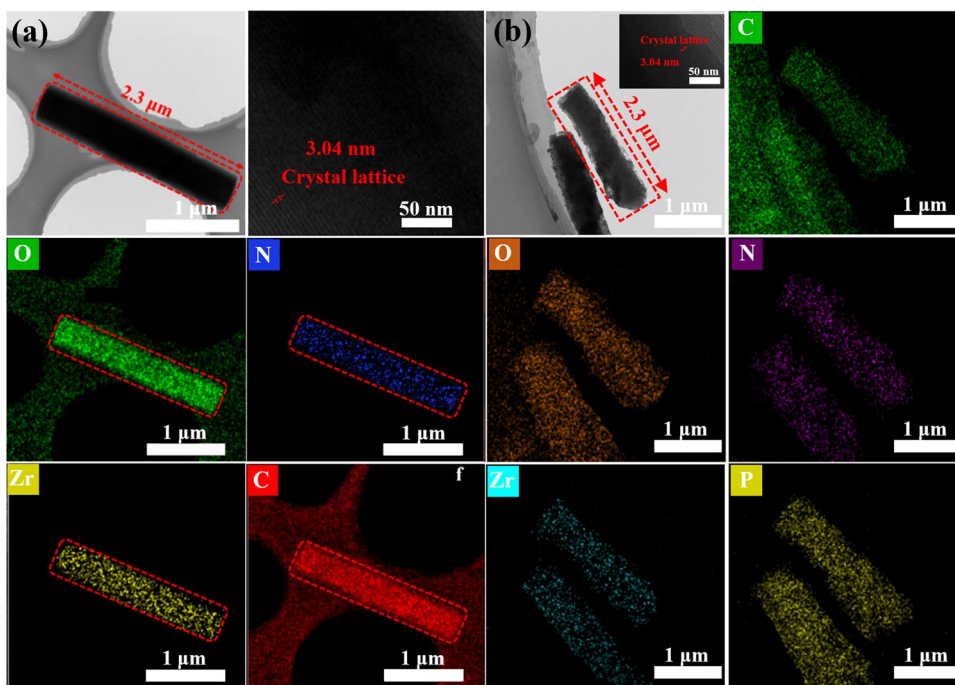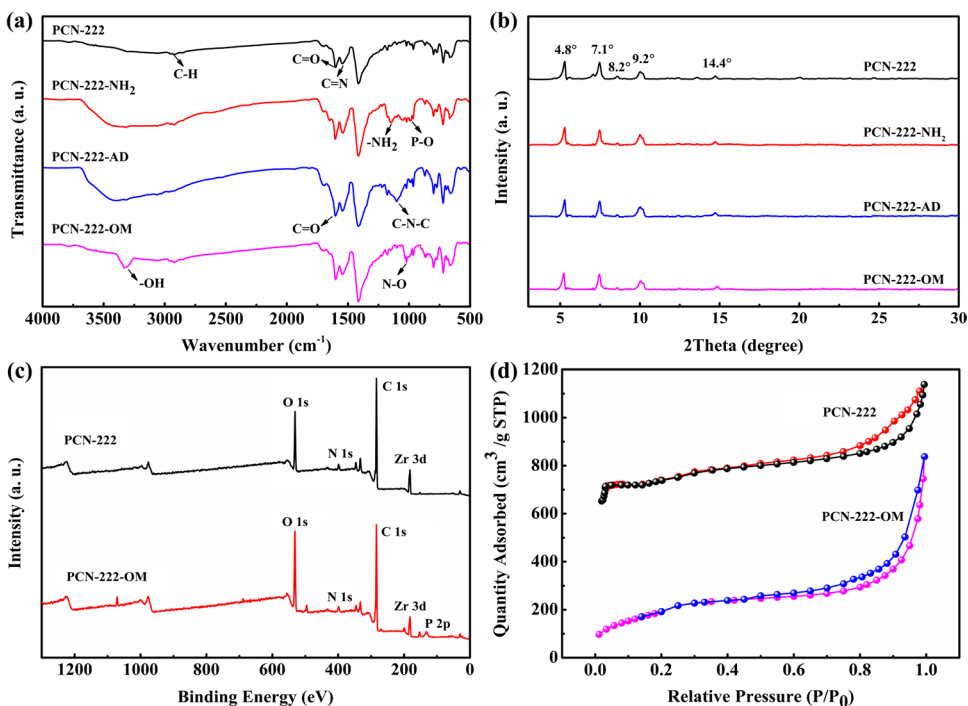
Fig. 3 The chemical structure characterizations of PCN-222-OM and its intermediates. **a** FT-IR. **b** XRD. **c** XPS. **d** N_2 adsorption–desorption isotherm

stationed at 2923, 1709, 1641, 1604, 1550, 1403, 965, 800, and 720 cm^{-1} severally, identical to literature data (Jia et al. 2019). After PCN-222 amination modification, two fresh peaks appeared at 1148 and 992 cm^{-1} on account of -NH$_2$ and P-O group stretching vibrations apart, evincing the -NH$_2$ groups which were triumphantly transplanted on PCN-222 (Bi et al. 2023). As far as PCN-222-AD was

concerned, the peak intensity of -NH$_2$ stretching vibration at 1148 cm^{-1} dropped and the one of C=O groups localized at 1603 cm^{-1} increased, and a fresh peak formed at 1101 cm^{-1} because of -C-N–C group stretching vibration, betokening a total transition from -C-NH$_2$ to -C-N–C, and PCN-222-AD was prepared (Sharma et al. 2005; Yamauchi et al. 2013). After the oximation modification, two fresh

peaks arose at 3328 and 1020 cm^{-1} in PCN-222-OM compared to PCN-222, owing to the stretching vibration of the associating -OH and N–O in C = N–OH groups (Mei et al. 2021).

XRD analysis

In Fig. 3b, several diffraction peaks were located at 2Theta of 4.8°, 7.1°, 8.2°, 9.2°, and 14.4° in PCN-222 XRD pattern, basically in accord with the literature data, proving the PCN-222 was successfully synthesized (Zhang et al. 2016). In comparison with PCN-222, the diffraction peak positions of PCN-222-OM and its intermediates were basically unchanged, demonstrating PCN-222 crystal structure was undamaged in multistep modifications.

XPS analysis

In order to prove that the oximation modification on PCN-222 was successful, the XPS analysis was conducted and the results are demonstrated in Fig. 3c. PCN-222 mainly comprised of C 1s, N 1s, O 1s, and Zr 3d. After oximation modification, PCN-222-OM mainly comprised of C 1s, O 1s, N 1s, P 2p, and Zr 3d. P element appearance was due to the use of aminomethylphosphonic acid modifier in the modification process. After the oxime modifications, the main introduced functional groups were C = N–OH groups, so the N 1s spectra were detailedly analyzed. As indicated in Fig. S1, three peaks in PCN-222 N 1s high-resolution spectrum originated from C = N groups (397.2

eV), C-N groups (399.4 eV), and -NH groups (401.3 eV) respectively (Yi et al. 2019; Guo et al. 2021). A novel peak at 399.3 eV after the oximation modification was the cause of newly generated C = N–OH groups (Zhu et al. 2022).

BET analysis

The evident hysteresis phenomena were observed in the adsorption/desorption isotherms of PCN-222 and PCN-222-OM (Fig. 3d), matching with archetypal type IV, demonstrating mesoporous structure came into existence in PCN-222 and PCN-222-OM (Liu et al. 2015; Bai et al. 2020b). The related parameters about adsorption/desorption isotherms are also summarized in the Table 1 and Fig. S2. Specific surface area and main pore size of PCN-222-OM were 1160 m^2·g^{-1} and 3.5 nm apart, which were smaller than those of PCN-222 (2546 m^2·g^{-1} and 3.7 nm) now that generated oxime groups occupied and blocked the pore space of PCN-222 (Wu et al. 2018; Amini et al. 2021). Although the introduction of oxime groups caused a fall for PCN-222 specific surface area and pore size, it was valuable for powerful adsorption.

## Uranium (VI) adsorption assay

pH effect

As seen from Fig. 4a, the pH values were highly influential in adsorption performance over PCN-222-OM and intermediates. PCN-222 adsorption capacity cumulated fleetly at pH = 2.0–4.0 and fell at pH = 4.0–10.0. PCN-222 maximum adsorption capacity was 361.4 mg·g^{-1}. Adsorption capacities of PCN-222-NH$_2$ and PCN-222-AD registered the same trends while pH values made changes. Their adsorption capacities increased largely at pH = 2.0–5.0 and afterwards fell throughout pH = 5.0–10.0. The maximum adsorption capacity of PCN-222-NH$_2$ and PCN-222-AD was 314.5 and 306.1 mg·g^{-1} at pH = 5.0 apart. PCN-222-OM maximum adsorption capacity was 403.4 mg·g^{-1} at pH = 6.0, much larger than its intermediates. Moreover, the main

Table 1 N$_2$ adsorption/desorption parameters of PCN-222 and PCN-222-OM

Sample	Specific surface area (m^2·g^{-1})	Main pore size (nm)
PCN-222	2546	3.7
PCN-222-OM	1160	3.5

Fig. 4 **a** Effect of pH value on the U(VI) adsorption capacities of PCN-222-OM and its intermediates (T = 25 ℃, t = 6 h, m/V = 0.2 g·L^{-1}, C_0 = 100 mg·L.$^{-1}$). **b** The distribution of U(VI) hydroxide species under different pH values (1–14)
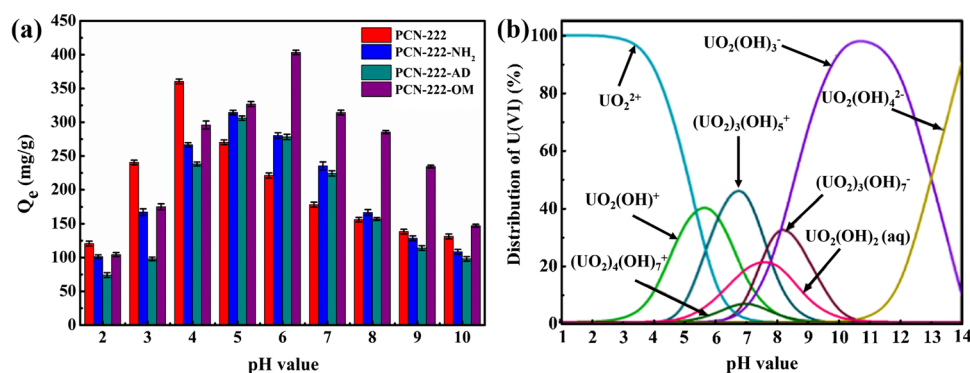
U(VI) existent forms within pH = 1.0–14.0 were investigated. In Fig. 4b, major species in U(VI) solution were UO_2^{2+}, $UO_2(OH)^+$, and $(UO_2)_3(OH)_5^+$ with positive charge at pH ≤ 7.0. With further increase of pH (7.0–10.0), the predominant U(VI) forms were $(UO_2)_3(OH)_7^-$, $UO_2(OH)_3^-$, and uranyl carbonates. Simultaneously, PCN-222 and PCN-222-OM zeta potential at pH = 2.0–10.0 was tested. PCN-222 had a positive surface charge below pH = 3.4 and a negative one at higher pH values (Fig. S3). The surface of PCN-222-OM was positively charged under pH = 5.2; nevertheless, its surface charge turned negative with pH value further rise. Therefore, there appeared a forceful repulsion between protonated PCN-222-OM and positive-charge U(VI) species in low pH range, resulting in poor adsorption capacity under low pH (Zhang et al. 2005). Progressive deprotonation of the oxime groups with increasing pH values accounted for increasing adsorption capacity. Yet, PCN-222-OM adsorption capacity dwindled as pH value appreciated to larger degrees as PCN-222-OM surface charge turned positive into negative, creating a big electrostatic repulsion with electronegative U(VI) species at high pH (Li et al. 2015). Briefly, PCN-222-OM superlative adsorption pH value was 6.0 and maximum adsorption capacity was 403.4 mg·g^{-1}.

Adsorbent dosage effect

Considering U(VI) removal rate and cost performance, it was crucial to find the best adsorbent dosage. In our exploration, various PCN-222-OM dosages (m/V = 0.05–0.3 g·L^{-1}) were placed inside 50 mL solution with 100 mg·L^{-1} original concentration. In Fig. 5, adsorption capacity was eroded with a constant increase in PCN-222-OM dosage. PCN-222-OM adsorption capacities were 596.6 and 273.2 mg·g^{-1}

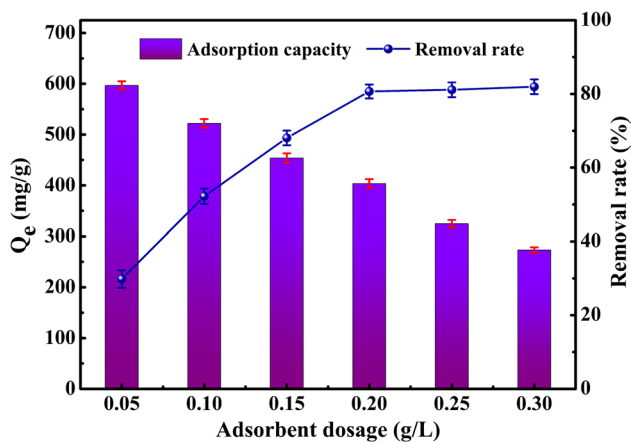at m/V = 0.05 and 0.3 g·L^{-1} apart. Additionally, removal rate boosted swiftly with PCN-222-OM dosage increase and almost remained unchanged at m/V = 0.2 g·L^{-1}. This reason for changing trends was that adsorption site quantities rose with constant increase in PCN-222-OM dosage when the m/V value was under 0.2 g·L^{-1}. However, a big competitive effect and spatial site resistance between adsorbents caused difficulty binding PCN-222-OM and U(VI) ions together at m/V > 0.2 g·L^{-1}, so further increasing PCN-222-OM dosage could not help to significantly improve its U(VI) removal rate (Wang and Guo 2020; Zhu et al. 2021a). Fig. S4 illustrates the influence of PCN-222 dosage upon its adsorption ability and removal rate, which had identical trend with PCN-222-OM. Therefore, m/V = 0.2 g·L^{-1} was nominated as adsorbent dosage during the following tests.

Adsorption isotherms

The adsorption capacities and removal rates of PCN-222 and PCN-222-OM at divergent initial U(VI) concentrations (C_0) were explored. In Fig. 6, adsorption capacities increased rapidly with C_0 rise. The growth rate of adsorption capacity was greater below C_0 = 100 mg·L^{-1}. Afterwards, it decreased above C_0 = 100 mg·L^{-1}, which proved adsorption processes of PCN-222 and PCN-222-OM achieved balances. Additionally, the maximum removal rates over PCN-222 and PCN-222-OM were 56.8% and 92.0% at C_0 = 0.5 mg·L^{-1} accordingly, which progressively fell with C_0 further increase. The removal rate dropped dramatically in C_0 = 100–200 mg·L^{-1}, presumably because PCN-222 and PCN-222-OM adsorption processes reached saturation (Dan et al. 2016).

Langmuir and Freundlich models, illustrated as Eqs. (S3–S4), were also applied to clarify adsorption processes of PCN-222 and PCN-222-OM. Involved constants are
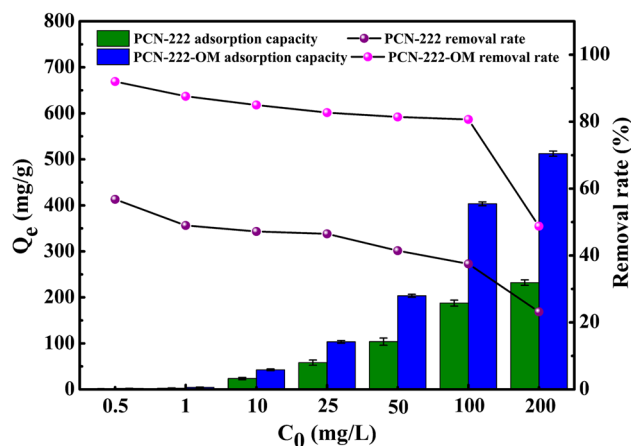
Fig. 5 Effect of PCN-222-OM dosage on the U(VI) adsorption capacity and removal rate (T = 25 ℃, t = 6 h, V = 50 mL, C_0 = 100 mg·L.$^{-1}$, pH = 6.0)

Fig. 6 Effect of initial concentration on the U(VI) adsorption capacity and removal rate of PCN-222 and PCN-222-OM (T = 25 ℃, t = 6 h, m/V = 0.2 g·L^{-1}, pH = 6.0)

summarized in Table 2. As for PCN-222-OM, the R^2 values of Langmuir and Freundlich models were 0.991 and 0.984 at 25 ℃ singly. Langmuir model's R^2 value was bigger than Freundlich model's, denoting monolayer adsorption brought U(VI) adsorption process under control. Furthermore, the Langmuir model ($R^2 = 0.995$) of PCN-222 was more fit than the Freundlich model ($R^2 = 0.985$), saying the PCN-222 adsorption process was also a monolayer adsorption (Chen et al. 2021).

Adsorption kinetics

With an advance of contact time, adsorption capacities for PCN-222 and PCN-222-OM considerably escalated and attained equilibrium at 360 min (Fig. 7a). The maximum adsorption capacities for PCN-222 and PCN-222-OM were 221.5 and 403.4 mg/g separately. Pseudo-first-order and pseudo-second-order models (Eqs. (S8–S9)) were put into practice to explore mechanisms. Simultaneously, correlative coefficients are also generalized in Table 3, which demonstrated pseudo-second-order model ($R^2_{PCN-222} = 0.965$, $R^2_{PCN-222-OM} = 0.992$) more precisely abided by the data than

the other model ($R^2_{PCN-222} = 0.819$, $R^2_{PCN-222-OM} = 0.876$), proving the chemical adsorption was a controllable step in PCN-222 and PCN-222-OM adsorption processes (Shi et al. 2020).

Adsorption thermodynamics

In Fig. 8, adsorption capacities of PCN-222 and PCN-222-OM progressively aggrandized as the temperature went up, proving the high temperature was valuable for PCN-222-OM adsorption (Xie et al. 2017). Thermodynamic parameters are numerated by Eqs. (S5–S7) and recorded in Table S1. Positive ΔH and ΔS values indicated the process was endothermic and randomness increased within solid-solution interface (Liu et al. 2018). When temperatures increased, the ΔG values turned more negative, demonstrating a spontaneous process (Akkaya 2013).

Selectivity of PCN-222-OM

U(VI) selectivity of PCN-222-OM was explored in complex multiple-metal-ion environment. The primary

Table 2 Langmuir and Freundlich isotherm parameters for U(VI) adsorption on PCN-222 and PCN-222-OM ($C_0 = 100$ mg·L^{-1}, $T = 25$ ℃, $m/V = 0.2$ g·L^{-1}, pH = 6.0)

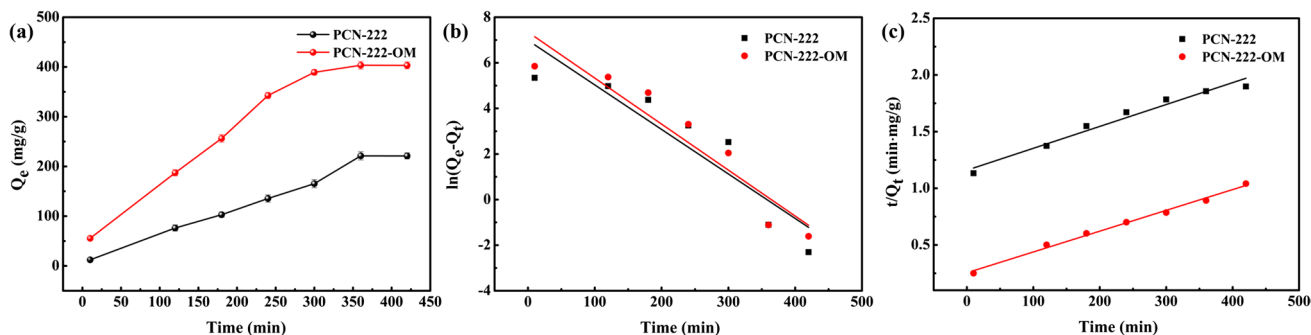| Sample	Langmuir model			Freundlich model		
	Q_m (mg·g^{-1})	K_L (L·mg^{-1})	R^2	K_F (mg·g^{-1})·(L·mg^{-1})$^{1/n}$	n	R^2
PCN-222	97.7	0.067	0.995	$e^{1.66}$	1.199	0.985
PCN-222-OM	238.5	0.240	0.991	$e^{3.37}$	1.262	0.984

Fig. 7 **a** Effect of contact time on the U(VI) adsorption capacities of PCN-222 and PCN-222-OM. **b** Pseudo-first-order model fitting curve. **c** Pseudo-second-order model fitting curve ($T = 25$ ℃, $C_0 = 100$ mg·L^{-1}, $m/V = 0.2$ g·L.$^{-1}$, pH = 6.0)

Table 3 Pseudo-first-order kinetic and pseudo-second-order kinetic coefficients for U(VI) adsorption on PCN-222 and PCN-222-OM ($C_0 = 100$ mg·L^{-1}, $m/V = 0.2$ g·L^{-1}, pH = 6.0, $T = 25$ ℃)

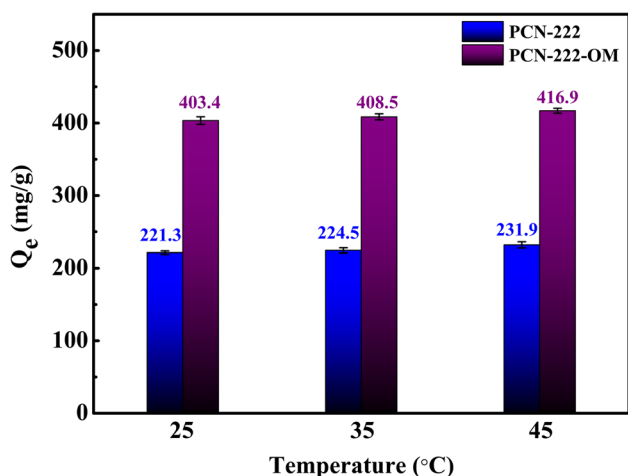| Sample	Pseudo-first-order			Pseudo-second-order		
	Q_e (mg·g^{-1})	k_1 (min^{-1})	R^2	Q_e (mg·g^{-1})	k_1 (g·mg^{-1}·min^{-1})	R^2
PCN-222	1085.8	0.019	0.819	518.1	3.2×10^{-6}	0.965
PCN-222-OM	1556.2	0.021	0.876	543.5	1.3×10^{-5}	0.992

Fig. 8 Effect of adsorption temperature on U(VI) adsorption capacities of PCN-222 and PCN-222-OM ($t = 6$ h, $C_0 = 100$ mg·L^{-1}, $m/V = 0.2$ g·L.$^{-1}$, pH = 6.0)
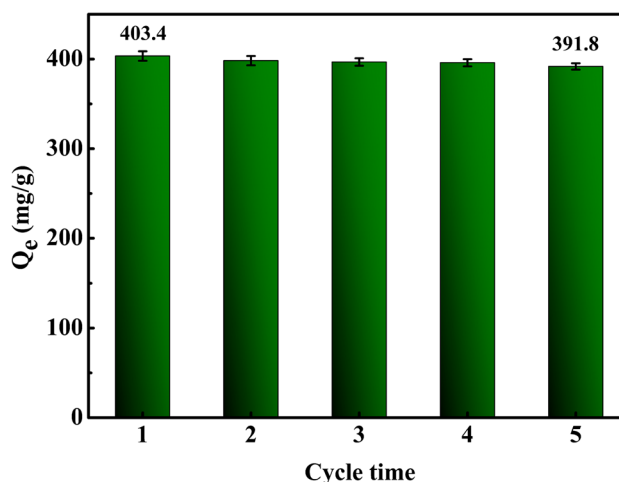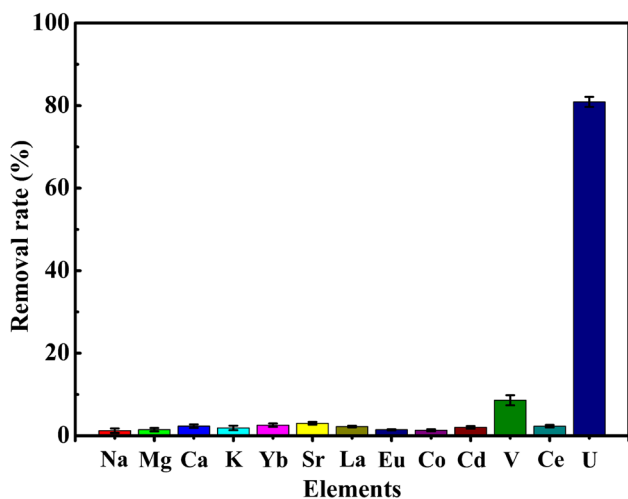

Fig. 9 Effect of co-existing cations on the U(VI) removal rate of PCN-222-OM ($T = 25$ ℃, $C_{\text{single cation}} = 10$ mg·L^{-1}, $m/V = 0.2$ g·L.$^{-1}$, pH = 6.0, $t = 6$ h)

Fig. 10 The recyclability of PCN-222-OM in the U(VI) adsorption ($T = 25$ ℃, $C_0 = 100$ mg·L^{-1}, $m/V = 0.2$ g·L.$^{-1}$, pH = 6.0, $t = 6$ h)

which also reflected the excellent U(VI) selectivity of PCN-222-OM.

Recyclability of PCN-222-OM

For continuable development, the recyclability of PCN-222-OM was explored. The experimental procedures about recyclability are itemized in supplemental file. In Fig. 10, the adsorption capacity declined only marginally in the fifth cycle in comparison with the first cycle. PCN-222-OM adsorption capacity still remained 391.8 mg·g^{-1} in the fifth cycle, demonstrating the eminent U(VI) recyclability of PCN-222-OM. Meanwhile, XRD and TEM results (Figs. S6 and S7) revealed that PCN-222-OM-U crystalline and morphology were well maintained through adsorption, reflecting marvelous stability and recyclability of PCN-222-OM.

Simulated nuclear industry wastewater test

For evaluating U(VI) selectivity of PCN-222-OM, simulated nuclear industrial waste samples of different U(VI) concentrations were prepared in accordance with a report about fuel-element-plant wastewater (Table S2). As illustrated in Fig. 11, PCN-222-OM possessed excellent U(VI) adsorption performances in the simulated fuel-element-plant wastewater samples of dissimilar U(VI) concentrations (10, 50, and 500 μg/L) and removal rates accomplished 48.0%, 54.2%, and 78.6% respectively, which proved the PCN-222-OM was prospective U(VI) adsorbent in complex nuclear industry wastewater.

Adsorption mechanism

Various characterizations were used for reconnoitering PCN-222-OM adsorption mechanism. In Fig. S6, PCN-222-OM

concentrations of applied co-existing cations were all 10 mg·L^{-1}. PCN-222-OM possessed very high U(VI) selectivity when other cations were co-existing (Fig. 9). PCN-222-OM owned still higher removal rate for U(VI) ions (80.9%) than for other cations, proving PCN-222-OM had the highest U(VI) selectivity. Meanwhile, the influences of various co-existing anions (NO$_3^-$, CO$_3^{2-}$, PO$_4^{3-}$, and SO$_4^{2-}$) on U(VI) removal rate were also under investigation and results are evinced in Fig. S5. The presence of anions brought about little impact upon U(VI) removal rate for PCN-222-OM,
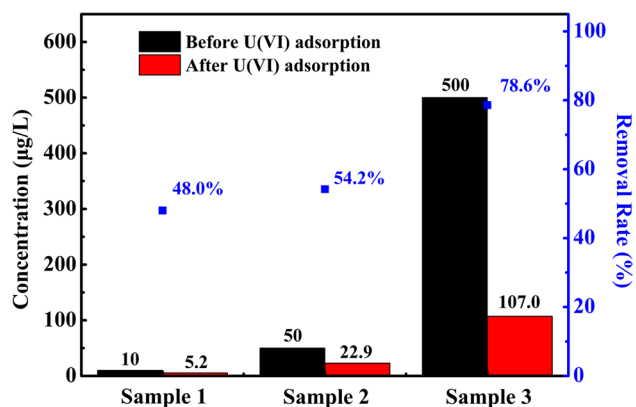
Fig. 11 The U(VI) adsorption performance of PCN-222-OM from simulated nuclear industry wastewater samples with different U(VI) concentrations (10, 50, and 500 μg·L.$^{-1}$)

XRD diffraction pattern remained essentially unchanged through U(VI) adsorption, manifesting crystalline structure did not show any considerable change in adsorption. As described in the FT-IR spectra (Fig. S8), compared with the original PCN-222-OM, the PCN-222-OM-U showed a characteristic vibration of O=U=O at 927 cm^{-1}, probably because of the interaction between the adsorption active sites and U(VI) ions. Furthermore, the XPS spectra and adsorption energy simulation calculations were carried out for elucidation adsorption mechanism of PCN-222-OM in depth. Figure 12a emerged the U 4f peaks arose through

PCN-222-OM U(VI) adsorption, which could be farther diverged into miscellaneous peaks. Two peaks in the U 4f high-resolution spectrum for PCN-222-OM-U were ascribed to U 4f$_{5/2}$ (392.9 eV) and U 4f$_{7/2}$ (382.1 eV), demonstrating PCN-222-OM successfully sorbed U(VI) ions (Perry 2015). Meanwhile, four peaks manifested in N 1s high-resolution spectrum for PCN-222-OM (Fig. 12c) were C=N (H$_2$TCPP) (397.2 eV), C-N (399.3 eV), C=N–OH (399.4 eV), and -NH (401.6 eV). After adsorption equilibrium, binding energy position for C=N–OH and -NH migrated approximately 1.6 eV and 0.3 eV apart, indicating C=N–OH and -NH groups were essential within adsorption process.

Meanwhile, adsorption energy calculations were carried out to explore interactions between functional groups within PCN-222-OM and U(VI) ions. Grounded on XPS analysis, C=N–OH and -NH groups were studied. In Fig. 13, their adsorption energies to U(VI) ions were −9.527 eV and −4.674 eV severally. In comparison with the -NH groups, the C=N–OH groups had stronger adsorption energy, proving they were dominating adsorption sites to U(VI) ions in PCN-222-OM. The -NH groups were secondary adsorption sites in the adsorption process of PCN-222-OM.

Antimicrobial activity appraisement

Minimum inhibitory concentration (MIC)

The antimicrobial activities for PCN-222-OM against *E. coli* and *S. aureus* were assessed via MIC tests. Bacterial

Fig. 12 **a** The full-scale XPS spectra of PCN-222-OM before and after U(VI) adsorption. **b** U 4f spectrum of PCN-222-OM after U(VI) adsorption. (**c**) N 1s spectrum of PCN-222-OM before U(VI) adsorption. (**d**) N 1s spectrum of PCN-222-OM after U(VI) adsorption
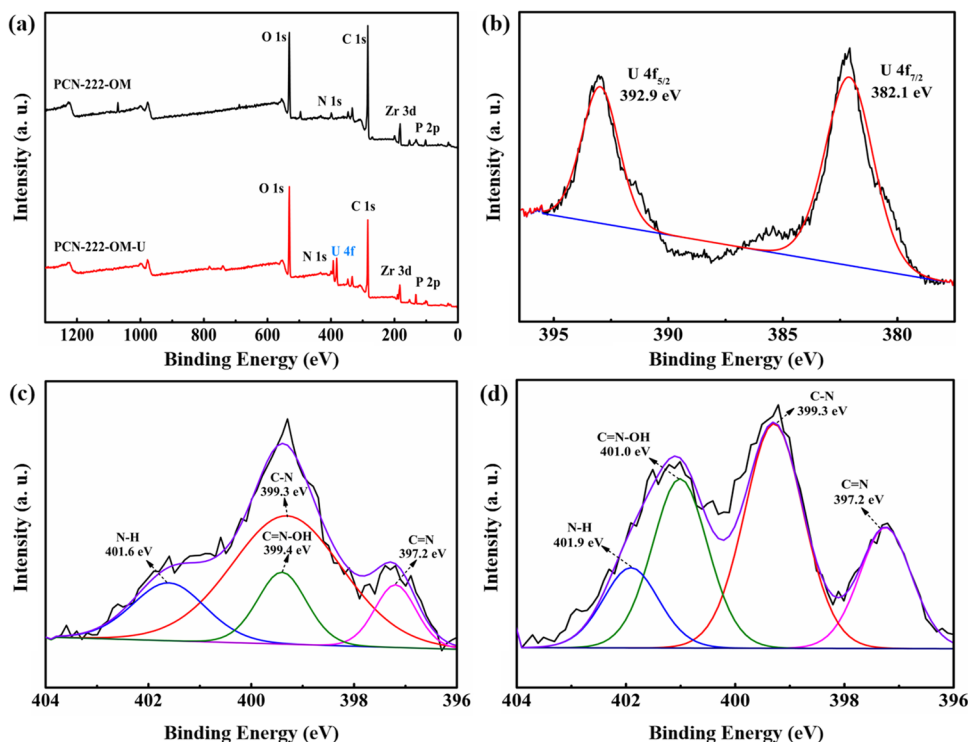
Fig. 13 Adsorption energy calculations between U(VI) ions and multifarious functional groups in PCN-222-OM (**a**) C=N–OH groups and (**b**) -NH groups
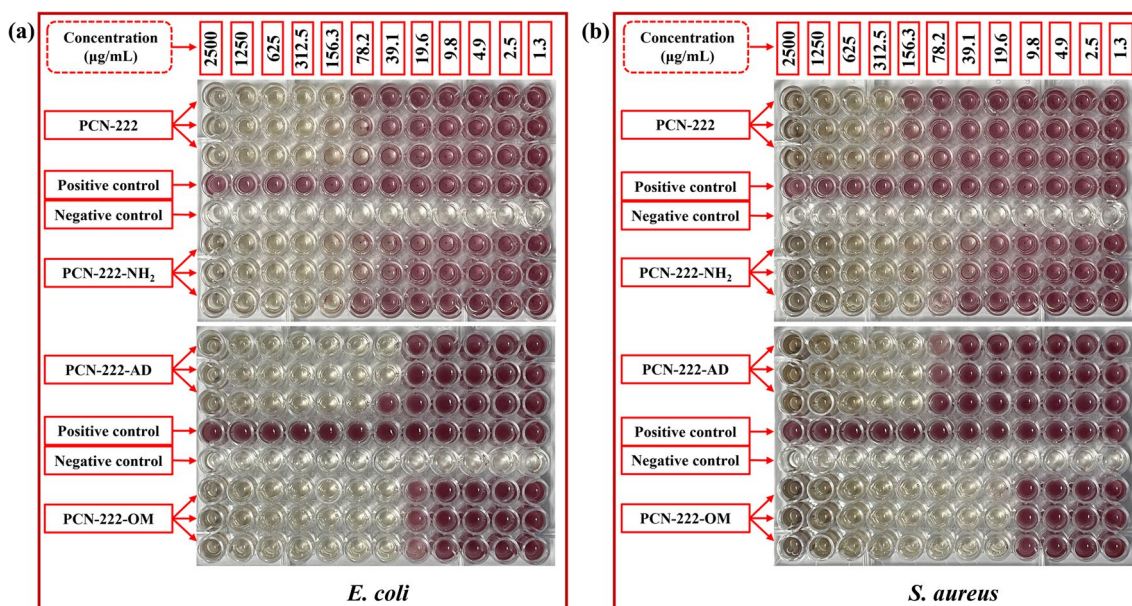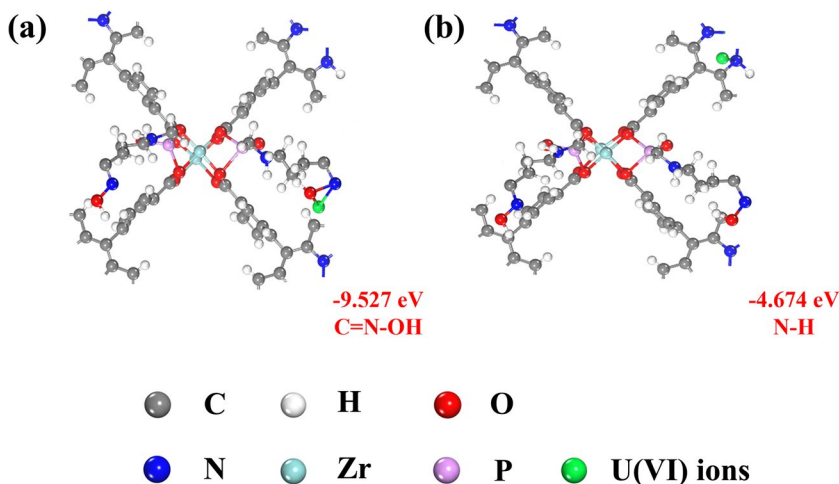

Fig. 14 The MIC values of PCN-222-OM and its intermediates against **a** *E. coli* and **b** *S. aureus*

suspension and solvent of the selfsame concentration were regarded as positive and negative control correspondingly. Figure 14 demonstrates that PCN-222-OM had evidence about great antimicrobial activity against *E. coli* and *S. aureus*. MIC values of PCN-222-OM against *E. coli* and *S. aureus* were 39.1 and 19.6 µg·mL^{-1} accordingly, evincing the outstanding antimicrobial activities of PCN-222-OM, providing assurance for efficient U(VI) extraction from complex environments.

Inhibition zone test

As displayed in Fig. 15, most samples possessed significant inhibition zones against *E. coli* and *S. aureus* after a 24-h incubation. PCN-222-OM zone diameters for *E. coli*

and *S. aureus* were 15.9 and 14.1 mm apart. By contrast, PCN-222-NH$_2$ and PCN-222-AD had larger inhibiting zones against *E. coli* and *S. aureus* than PCN-222, demonstrating introduced functional groups could improve the antimicrobial activity and permeability to a certain extent. Simultaneously, PCN-222-OM possessed the largest inhibition zone diameters compared with other intermediates, demonstrating its eminent permeabilities and antimicrobial activities over *E. coli* and *S. aureus*.

Inhibition of bacterial growth

PCN-222-OM inhibitions against *E. coli* and *S. aureus* multiplication were evaluated via OD$_{600}$ values within different dosage concentrations (20–320 µg·mL^{-1}).
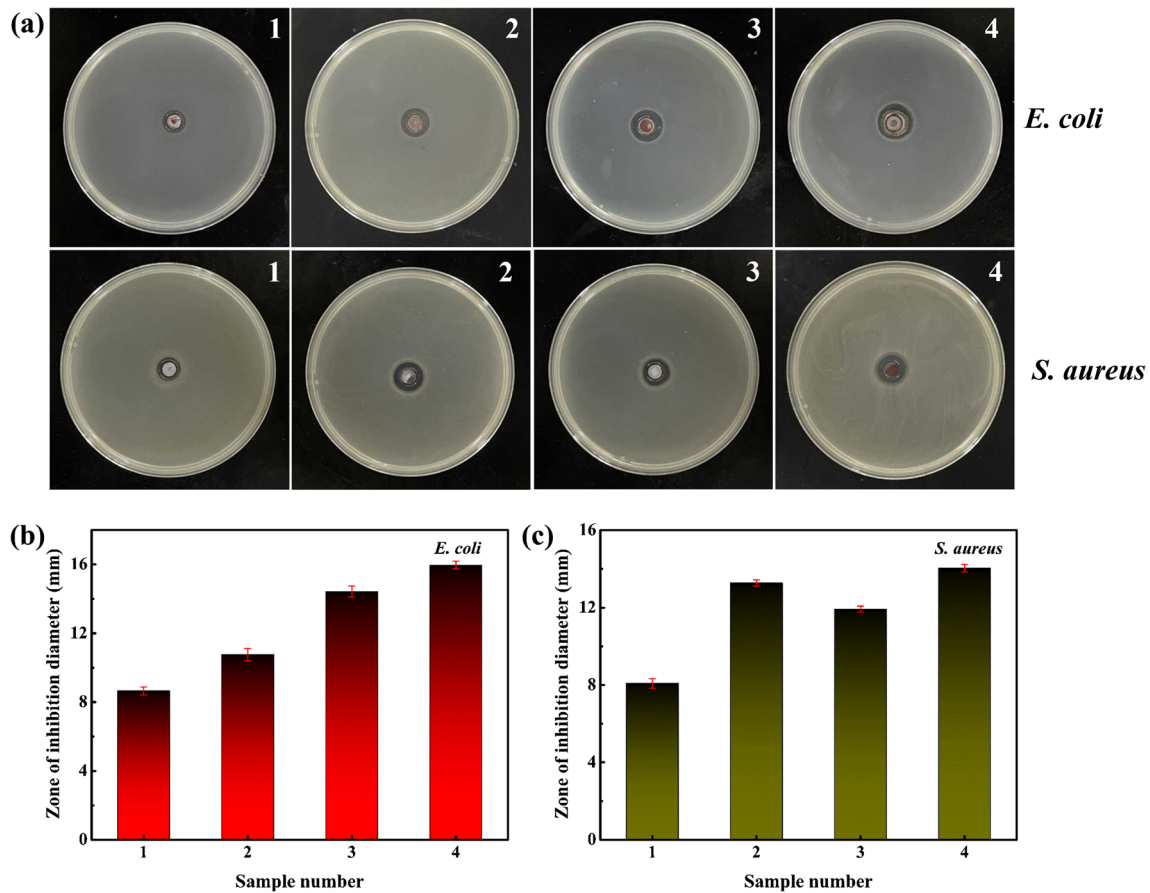
Fig. 15 The inhibition zone determinations of PCN-222-OM and its intermediates against *E. coli* and *S. aureus*. **a** Images of punch well agar diffusion test. (**b**, **c**) Zone of inhibition diameters against *E. coli* and *S. aureus* apart (sample 1 = PCN-222, sample 2 = PCN-222-NH$_2$, sample 3 = PCN-222-AD, and sample 4 = PCN-222-OM)

Fig. 16 The bacterial growth curves treated with PCN-222-OM against **a** *E. coli* and **b** *S. aureus*
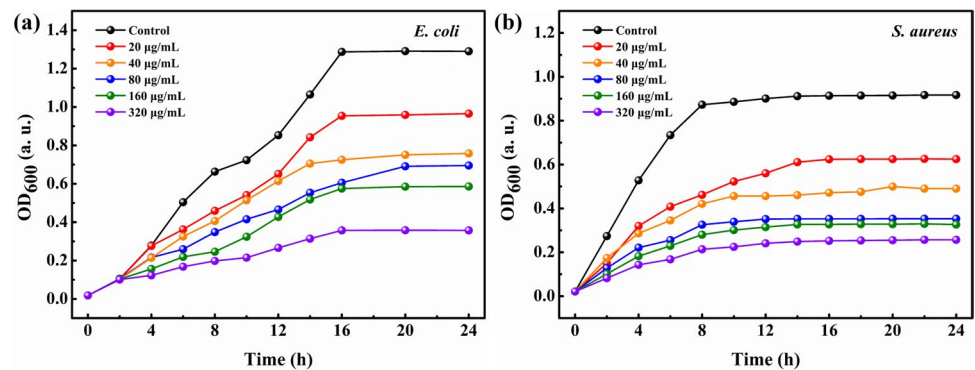
Lower OD$_{600}$ values indicated lower bacterial concentrations and better antimicrobial activity. As seen from Fig. 16, there were no significant inhibitions against *E. coli* and *S. aureus* build-up while the PCN-222-OM concentration was below 20 μg·mL^{-1}. PCN-222-OM did not produce significant inhibitions against *E. coli* and *S. aureus* multiplication until concentration range further increased to 40–160 μg·mL^{-1}. Subsequently, they nearly

stopped growing until the concentration was increased to 320 μg·mL^{-1}. Bacteria growth curves proved that the PCN-222-OM had good antibacterial property as the concentration was high enough. Meanwhile, Fig. S9 was the SEM image of *E. coli* and *S. aureus* around PCN-222-OM treating *E. coli* and *S. aureus*. Their surfaces were partially damaged throughout PCN-222-OM treating, possibly because of the interaction between the

$Zr_6(\mu_3\text{-}O)_4(\mu_3\text{-}OH)_4(H_2O)_4(OH)_4$ clusters and bacterial membrane.

Environmental safety and antibiofouling activity

Environmental safety

It is very momentous for environmental safety of adsorbents in practical adsorption. The minnow viability experiments were made to appraise the environmental and biological hazards from PCN-222-OM. As illustrated in Fig. S10, all minnows kept excellent zoological activities through 48-h PCN-222-OM treatment, proving PCN-222-OM had splendid environmental safety.

Antibiofouling activity

In general, the biological contamination showed significant impacts on U(VI) adsorbent capability. *Halamphora* was used to assess PCN-222-OM antibiofouling activity. In Fig. S11(a), PCN-222-OM had great inhibition against *Halamphora* growth and cell mortality nearly achieved 81.3% a week later, possibly because of the synergistic role of $Zr_6(\mu_3\text{-}O)_4(\mu_3\text{-}OH)_4(H_2O)_4(OH)_4$ clusters and affluent

groups within PCN-222-OM. Biological colonization on the adsorbent surface was also a major contributor to biological contamination. *Halamphora* cell viabilities are also investigated in Fig. S11(b). The minority of viable cells were noticed on PCN-222-OM surface a week later, demonstrating the PCN-222-OM could kill *Halamphora* cells as well as inhibit the adhesion.

Contrast about adsorption capacity and antimicrobial activity between PCN-222-OM and reported adsorbents

As illustrated in Table 4, PCN-222-OM was in possession of conspicuously finer adsorption capacity (403.4 mg·g^{-1}) in proportion to already reported adsorbents, such as ZIF-90-AO, MOF-5, UiO-66-NH$_2$, UiO-66-AO, and MIL-101 PCN-222-OM was a heartening U(VI) adsorbent. Meanwhile, the antimicrobial activity was also vital to sufficiently utilise the porous adsorbent performance. In Table 5, MICs of PCN-222-OM against *E. coli* and *S. aureus* were 39.1 and 19.6 μg·mL^{-1} severally, smaller than other adsorbents, which certified the antimicrobial activities of PCN-222-OM against *E. coli* and *S. aureus* were superior to reported absorbents.

Table 4 Contrast of U(VI) absorption capacity between PCN-222-OM and reported adsorbents

Absorbents	Experimental conditions	Q_e^{max} (mg·g^{-1})	References
ZIF-90-AO	pH = 5.0, C_0 = 100 mg·L^{-1}	382.5	Mei et al. 2022
MOF-5	pH = 5.0, C_0 = 300 mg·L − 1	237.0	Wang and Guo 2020
UiO-66-NH$_2$	pH = 5.5, C_0 = 100 mg·L^{-1}	115.0	Luo et al. 2016
UiO-66-AO	pH = 5.5, C_0 = 160 mg·L^{-1}	194.8	Liu et al. 2019
MIL-101	pH = 6.0, C_0 = 100 mg·L^{-1}	91.0	Liu et al. 2020b
MIL-101-ED	pH = 5.5, C_0 = 100 mg·L^{-1}	200.0	Bai et al. 2015
MOF-76	pH = 3.0, C_0 = 140 mg·L^{-1}	298.0	Yang et al. 2013
ZIF-8	pH = 4.5, C_0 = 80 mg·L^{-1}	64.9	Zhang et al. 2019b
PCN-222-OM	pH = 6.0, C_0 = 100 mg·L^{-1}	403.4	This study

Table 5 Contrast about antimicrobial activity between PCN-222-OM and reported adsorbents

Antimicrobial agents	Bacterial species	MIC (μg·mL^{-1})	References
ZIF-90-AO	*E. coli*	250	Mei et al. 2022
UiO-66-NH$_2$	*E. coli*	Infinite	Zhu et al. 2021b
MIL-101	*E. coli*	40,000	Hajibabaei et al. 2020
MOF-5	*E. coli*	200	Bhardwaj et al. 2018
ZIF-8	*E. coli*	256	Wang et al. 2016
PCN-222-OM	*E. coli*	39.1	This study
ZIF-90-AO	*S. aureus*	62.5	Mei et al. 2022
UiO-66-NH$_2$	*S. aureus*	Infinite	Zhu et al. 2021b
MIL-101	*S. aureus*	80,000	Hajibabaei et al. 2020
MOF-5	*S. aureus*	200	Bhardwaj et al. 2018
ZIF-8	*S. aureus*	256	Wang et al. 2016
PCN-222-OM	*S. aureus*	19.6	This study

To sum up, PCN-222-OM was one golden U(VI) adsorbent due to eminent adsorption capacity and antimicrobial activity.

Conclusion

One newfangled and efficient U(VI) adsorbent named PCN-222-OM with glorious antimicrobial activity, environmental safety, and antibiofouling activity was designed and synthesized grounded on PCN-222 directed molecular structure design. PCN-222-OM possessed outstanding U(VI) adsorption capacity at a maximum of 403.4 mg·g^{-1} at pH = 6.0, owing to interactions between U(VI) ions and abundant porous structures and oxime groups in PCN-222-OM. Meanwhile, PCN-222-OM also displayed splendid recyclability and selectivity in U(VI) adsorption, whose selective removal rate was 78.6% in the simulated nuclear industry wastewater with 500 µg/L U(VI) concentration. Kinetic and isothermal constants attested that PCN-222-OM adsorption process was predominantly in the charge of chemisorption and monolayer adsorption. XPS spectra and adsorption energy calculation results proved C = N–OH and -NH groups occupied key roles during the adsorption process and adsorption mechanism was considered to have synergy function about coordination and electrostatic interaction. PCN-222-OM presented eminent antimicrobial activity against *E. coli* and *S. aureus* due to the interaction between $Zr_6(\mu_3\text{-O})_4(\mu_3\text{-OH})_4(H_2O)_4(OH)_4$ clusters and bacterial membrane, which effectively reduced the damaging impact from bacteria upon U(VI) adsorption capacity. Meanwhile, PCN-222-OM disclosed fine environmental safety and antibiofouling activity, avoiding side impact about biological contamination on U(VI) adsorption capacity and meeting non-toxicity request in applications. In summary, PCN-222-OM became an inspiriting adsorbent in wastewater U(VI) recovery and engendered one valuable thought for effective adsorbent advancement.

The recommendations for future work

In comparison with the reported U(VI) adsorbents, the synthesized PCN-222-OM has a number of characteristic advantages in adsorption performance. Although PCN-222-OM has the advantages in large adsorption capacity, high adsorption efficiency, strong selective adsorption ability, strong resistance to biological contamination, and easy recycling, it still has a lot of room for improvement in the future work. On the one hand, in order to advance the practical engineering application of U(VI) adsorbents, the cost consumption in the preparation of U(VI) adsorbents can be further reduced in future research work. The preparation of MOF-based U(VI) adsorbents can be conducted with simpler group modification methods in future work. On the other hand, it is best to use real nuclear industrial waste samples in the possible future adsorption performance test work to make the adsorption performance results closer to the actual application.

Author contribution Changlong Bi: writing original draft, validation, formal analysis, and investigation.

Chunhong Zhang: conceptualization, methodology, validation, investigation, resources, writing, review, editing, supervision, and project administration.

Chao Wang: validation, formal analysis, methodology, resources, and supervision.

Lien Zhu: validation, formal analysis, software, and visualization.

Ruiqi Zhu: validation, formal analysis, and software.

Lijia Liu: validation, formal analysis, software, methodology, and visualization.

Yudan Wang: validation, formal analysis, methodology, resources, and supervision.

Fuqiu Ma: validation, formal analysis, methodology, and supervision.

Hongxing Dong: resources, project administration, and formal analysis.

All the authors listed have approved this manuscript.

Data availability All data generated or analyzed during the study have been included in this manuscript and its supplementary information files.

Declarations

Ethical approval Not applicable.

Consent for publication This manuscript is approved by all authors for publication in Environmental Science and Pollution Research.

Competing interests The authors declare no competing interests.

References

Aguado S, Quiros J, Canivet J, Farrusseng D, Boltes K, Rosal R (2014) Antimicrobial activity of cobalt imidazolate metal-organic frameworks. Chemosphere 113:188–192. https://doi.org/10.1016/j.chemosphere.2014.05.029

Akkaya R (2013) Removal of radioactive elements from aqueous solutions by adsorption onto polyacrylamide-expanded perlite: equilibrium, kinetic, and thermodynamic study. Desalination 321:3–8. https://doi.org/10.1016/j.desal.2012.09.020

Amini A, Khajeh M, Oveisi AR, Daliran S, Ghaffari-Moghaddam M, Delarami HS (2021) A porous multifunctional and magnetic layered graphene oxide/3D mesoporous MOF nanocomposite for rapid adsorption of uranium(VI) from aqueous solutions. J Ind Eng Chem 93:322–332. https://doi.org/10.1016/j.jiec.2020.10.008

Anirudhan TS, Jalajamony S (2013) Ethyl thiosemicarbazide intercalated organophilic calcined hydrotalcite as a potential sorbent for the removal of uranium(VI) and thorium(IV) ions from aqueous solutions. J Environ Sci 25:717–725. https://doi.org/10.1016/S1001-0742(12)60064-3

Arica MY, Bayramoglu G (2016) Polyaniline coated magnetic carboxymethylcellulose beads for selective removal of uranium ions from aqueous solution. J Radioanal Nucl Chem 310:711–724. https://doi.org/10.1007/s10967-016-4828-z

Bai ZQ, Yuan LY, Zhu L, Liu ZR, Chu SQ, Zheng LR, Zhang J, Chai ZF, Shi WQ (2015) Introduction of amino groups into acid-resistant MOFs for enhanced U(VI) sorption. J Mater Chem A 3:525–534. https://doi.org/10.1039/c4ta04878d

Bai JW, Ma XF, Gong C, Chen YM, Yan HJ, Wang KW, Wang J (2020a) A novel amidoxime functionalized porous resins for rapidly selective uranium uptake from solution. J Mol Liq 320:114443. https://doi.org/10.1016/j.molliq.2020.114443

Bai ZH, Liu Q, Song DL, Zhang HS, Liu JY, Chen RR, Yu J, Li RM, Wang J (2020b) Preparation of a 3D multi-branched chelate adsorbent for high selective adsorption of uranium(VI): acrylic and diaminomaleonitrile functionalized waste hemp fiber. React Funct Polym 149:104512. https://doi.org/10.1016/j.reactfunctpolym.2020.104512

Bhardwaj N, Pandey SK, Mehta J, Bhardwaj SK, Kim KH, Deep A (2018) Bioactive nano-metal-organic frameworks as antimicrobials against Gram-positive and Gram-negative bacteria. Toxicol Res 7:931–941. https://doi.org/10.1039/c8tx00087e

Bi CL, Zhang CH, Ma FQ, Zhang X, Yang M, Nian JR, Liu LJ, Dong HX, Zhu LE, Wang Q, Guo SX, Lv QT (2021) Growth of a mesoporous Zr-MOF on functionalized graphene oxide as an efficient adsorbent for recovering uranium (VI) from wastewater. Microporous Mesoporous Mat 323:111223. https://doi.org/10.1016/j.micromeso.2021.111223

Bi CL, Zhang CH, Ma FQ, Zhu LE, Zhu RQ, Qi Q, Liu LJ, Dong HX (2022) Development of 3D porous $Ag^{(+)}$ decorated PCN-222 @ graphene oxide-chitosan foam adsorbent with antibacterial property for recovering U(VI) from seawater. Sep Purif Technol 281:119900. https://doi.org/10.1016/j.seppur.2021.119900

Bi CL, Zhang CH, Xu WD, Ma FQ, Zhu LE, Zhu RQ, Qi Q, Liu LJ, Bai JW, Dong HX (2023) Highly efficient antibacterial adsorbent for recovering uranium from seawater based on molecular structure design of PCN-222 post-engineering. Desalination 545:116169. https://doi.org/10.1016/j.desal.2022.116169

Carboni M, Abney CW, Liu SB, Lin WB (2013) Highly porous and stable metal-organic frameworks for uranium extraction. Chem Sci 4:2396–2402. https://doi.org/10.1039/c3sc50230a

Chen G, Weng HQ, Wu ZH, Chen YZ, Zhang P, Ye GA, Lin MZ (2021) High-yield production of monolayer boron nitride nanosheets by cationic-surfactant-assisted solvothermal exfoliation for the ultrafast and selective separation of U(VI) from lanthanides. Sep Purif Technol 278:119645. https://doi.org/10.1016/j.seppur.2021.119645

Chen F, Lv M, Ye Y, Miao SY, Tang X, Liu Y, Liang B, Qin ZM, ChenYL HZW, Wang YH (2022) Insights on uranium removal by ion exchange columns: the deactivation mechanisms, and an overlooked biological pathway. Chem Eng J 434:134708. https://doi.org/10.1016/j.cej.2022.134708

Damljanovic I, Vukicevic M, Vukicevic RD (2006) A simple synthesis of oximes. Mon Chem 137:301–305. https://doi.org/10.1007/s00706-005-0427-3

Dan H, Ding Y, Lu XR, Chi FT, Yuan SB (2016) Adsorption of uranium from aqueous solution by mesoporous SBA-15 with various morphologies. J Radioanal Nucl Chem 310:1107–1114. https://doi.org/10.1007/s10967-016-4865-7

El-Din AFT, El-Din EA, El-Din ME (2018) Cellulose acetate/EDTA-chelator assisted synthesis of ordered mesoporous HAp microspheres for efficient removal of radioactive species from seawater. J Environ Chem Eng 6:5845–5854. https://doi.org/10.1016/j.jece.2018.09.005

Feng D, Gu ZY, Li JR, Jiang HL, Wei Z, Zhou HC (2012) Zirconium metalloporphyrin PCN-222: mesoporous metal-organic frameworks with ultrahigh stability as biomimetic catalysts. Angew Chem Int Edit 51:10307–10310. https://doi.org/10.1002/anie.201204475

Guo Y, Zhang XY, Xie NY, Guo RX, Wang Y, Sun ZJ, Li H, Jia HN, Niu D, Sun HB (2021) Investigation of antimony adsorption on a zirconium-porphyrin-based metal-organic framework. Dalton Trans 50:13932–13942. https://doi.org/10.1039/d1dt01895g

Hajibabaei M, Zendehdel R, Panjali Z (2020) Imidazole-functionalized Ag/MOFs as promising scaffolds for proper antibacterial activity and toxicity reduction of Ag nanoparticles. J Inorg Organomet Polym Mater 30:4622–4626. https://doi.org/10.1007/s10904-020-01612-8

He T, Chen SM, Ni B, Gong Y, Wu Z, Song L, Gu L, Hu WP, Wang X (2018) Zirconium-porphyrin-based metal-organic framework hollow nanotubes for immobilization of noble-metal single atoms. Angew Chem-Int Edit 57:3493–3498. https://doi.org/10.1002/anie.201800817

Jia HJ, Ma DX, Zhong SW, Li LJ, Li L, Xu L, Li BY (2019) Boosting photocatalytic activity under visible-light by creation of PCN-222/g-C_3N_4 heterojunctions. Chem Eng J 368:165–174. https://doi.org/10.1016/j.cej.2019.02.147

Kandre S, Bhagat PR, Sharma R, Gupte A (2013) Microwave assisted synthesis of 3,5-disubstituted 1,2,4-oxadiazoles from substituted amidoximes and benzoyl cyanides. Tetrahedron Lett 54:3526–3529. https://doi.org/10.1016/j.tetlet.2013.04.101

Khedr MG (2015) Nanofiltration of oil field-produced water for reinjection and optimum protection of oil formation. Desalin Water Treat 55:3460–3468. https://doi.org/10.1080/19443994.2014.939497

Li L, Hu N, Ding DX, Xin X, Wang YD, Xue JH, Zhang H, Tan Y (2015) Adsorption and recovery of U(VI) from low concentration uranium solution by amidoxime modified aspergillus niger. RSC Adv 5:65827–65839. https://doi.org/10.1039/c5ra13516h

Li JQ, Gong LL, Feng XF, Zhang L, Wu HQ, Yan CS, Xiong YY, Gao HY, Luo F (2017a) Direct extraction of U(VI) from alkaline solution and seawater via anion exchange by metal-organic framework. Chem Eng J 316:154–159. https://doi.org/10.1016/j.cej.2017.01.046

Li P, Zhun B, Wang XG, Liao PP, Wang GH, Wang LZ, Guo YD, Zhang WM (2017b) Highly efficient interception and precipitation of uranium(VI) from aqueous solution by iron-electrocoagulation combined with cooperative chelation by organic ligands. Environ Sci Technol 51:14368–14378. https://doi.org/10.1021/acs.est.7b05288

Li J, Wu Z, Duan QY, Alsaedi A, Hayat T, Chen CL (2018) Decoration of ZIF-8 on polypyrrole nanotubes for highly efficient and selective capture of U(VI). J Clean Prod 204:896–905. https://doi.org/10.1016/j.jclepro.2018.09.050

Li H, Zhai FW, Gui DX, Wang XX, Wu CF, Zhang D, Dai X, Deng H, Su XT, Di-wu J, Lin Z, Chai ZF, Wang SA (2019) Powerful uranium extraction strategy with combined ligand complexation and photocatalytic reduction by postsynthetically modified photoactive metal-organic frameworks. Appl Catal B-Environ 254:47–54. https://doi.org/10.1016/j.apcatb.2019.04.087

Li FF, Cui WR, Jiang W, Zhang CR, Liang RP, Qiu JD (2020a) Stable sp(2) carbon-conjugated covalent organic framework for detection

and efficient adsorption of uranium from radioactive wastewater. J Hazard Mater 392:122333. https://doi.org/10.1016/j.jhazmat.2020.122333

Li P, Chen P, Wang GH, Wang LZ, Wang XG, Li YR, Zhang WM, Jiang H, Chen H (2020b) Uranium elimination and recovery from wastewater with ligand chelation-enhanced electrocoagulation. Chem Eng J 393:124819. https://doi.org/10.1016/j.cej.2020.124819

Li N, Yang L, Yang D, Tang CY, Deng WQ, Wang ZN (2021a) High-capacity amidoxime-functionalized beta-cyclodextrin/graphene aerogel for selective uranium capture. Environ Sci Technol 55:9181–9188. https://doi.org/10.1021/acs.est.0c08743

Li SS, Li QQ, Luo JQ, Shu YZ, Guo KX, Xie JX, Xiao FZ, He SY (2021b) Application progress of deinococcus radiodurans in biological treatment of radioactive uranium-containing wastewater. Indian J Microbiol 61:417–426. https://doi.org/10.1007/s12088-021-00969-9

Liang LL, Zhang H, Lin XY, Yan KY, Li MS, Pan XH, Hu Y, Chen Y, Luo XG, Shang R (2021) Phytic acid-decorated porous organic polymer for uranium extraction under highly acidic conditions. Colloid Surf A-Physicochem Eng Asp 625:126981. https://doi.org/10.1016/j.colsurfa.2021.126981

Lin K, Sun WY, Feng LJ, Wang H, Feng TT, Zhang JC, Cao M, Zhao SL, Yuan YH, Yuan N (2022) Kelp inspired bio-hydrogel with high antibiofouling activity and super-toughness for ultrafast uranium extraction from seawater. Chem Eng J 430:133121. https://doi.org/10.1016/j.cej.2021.133121

Liu GL, Wang YX, Shen CJ, Ju ZF, Yuan DQ (2015) A facile synthesis of microporous organic polymers for efficient gas storage and separation. J Mater Chem a 3:3051–3058. https://doi.org/10.1039/c4ta05349d

Liu SJ, Ouyang JX, Luo JQ, Sun L, Huang GL, Ma JG (2018) Removal of uranium (VI) from aqueous solution using graphene oxide functionalized with diethylenetriaminepentaacetic phenylenediamine. J Nucl Sci Technol 55:781–791. https://doi.org/10.1080/00223131.2018.1439415

Liu JM, Yin XH, Liu T (2019) Amidoxime-functionalized metal-organic frameworks UiO-66 for U(VI) adsorption from aqueous solution. J Taiwan Inst Chem Eng 95:416–423. https://doi.org/10.1016/j.jtice.2018.08.012

Liu LJ, Fang YG, Meng YJ, Wang XY, Ma FQ, Zhang CH, Dong HX (2020a) Efficient adsorbent for recovering uranium from seawater prepared by grafting amidoxime groups on chloromethylated MIL-101(Cr) via diaminomaleonitrile intermediate. Desalination 478:114300. https://doi.org/10.1016/j.desal.2019.114300

Liu S, Bai JL, Huo YP, Ning BA, Peng Y, Li S, Han DP, Kang WJ, Gao ZX (2020b) A zirconium-porphyrin MOF-based ratiometric fluorescent biosensor for rapid and ultrasensitive detection of chloramphenicol. Biosens Bioelectron 149:111801. https://doi.org/10.1016/j.bios.2019.111801

Liu C, Dong ZM, Yu CH, Gong JY, Gong YQ, Gong ZB, Liu YH (2021) Study on photocatalytic performance of hexagonal SnS_2/g-C_3N_4 nanosheets and its application to reduce U(VI) in sunlight. Appl Surf Sci 537:147754. https://doi.org/10.1016/j.apsusc.2020.147754

Liu XL, Xie YH, Hao MJ, Chen ZS, Yang H, Waterhouse GIN, Ma SQ, Wang XK (2022) Highly efficient electrocatalytic uranium extraction from seawater over an amidoxime-functionalized in-N-C catalyst. Adv Sci 9:2201735. https://doi.org/10.1002/advs.202201735

Luo BC, Yuan LY, Chai ZF, Shi WQ, Tang Q (2016) U(VI) capture from aqueous solution by highly porous and stable MOFs: UiO-66 and its amine derivative. J Radioanal Nucl Chem 307:269–276. https://doi.org/10.1007/s10967-015-4108-3

Ma FQ, Gui YY, Liu P, Xue Y, Song W (2020) Functional fibrous materials-based adsorbents for uranium adsorption and environmental

remediation. Chem Eng J 390:124597. https://doi.org/10.1016/j.cej.2020.124597

Mei DC, Li H, Liu LJ, Jiang LC, Zhang CH, Wu XR, Dong HX, Ma FQ (2021) Efficient uranium adsorbent with antimicrobial function: oxime functionalized ZIF-90. Chem Eng J 425:130468. https://doi.org/10.1016/j.cej.2021.130468

Mei DC, Liu LJ, Li H, Wang YD, Ma FQ, Zhang CH, Dong HX (2022) Efficient uranium adsorbent with antimicrobial function constructed by grafting amidoxime groups on ZIF-90 via malononitrile intermediate. J Hazard Mater 422:126872. https://doi.org/10.1016/j.jhazmat.2021.126872

Park J, Gill GA, Strivens JE, Kou LJ, Jeters RT, Avila A, Wood JR, Schlafer NJ, Janke CJ, Miller EA, Thomas M, Addleman RS, Bonheyo GT (2016) Effect of biofouling on the performance of amidoxime-based polymeric uranium adsorbents. Ind Eng Chem Res 55:4328–4338. https://doi.org/10.1021/acs.iecr.5b03457

Paz J, Perez-Balado C, Iglesias B, Munoz L (2010) Different reactivity of hydroxylamine with carbamoyl azides and carbamoyl cyanides: synthesis of hydroxyureas and carbamoyl amidoximes. J Org Chem 75:8039–8047. https://doi.org/10.1021/jo1014855

Perry DL (2015) The tris(carbonato)dioxouranium(VI) ion: a structural model for uranium 4f(7/2), (5/2) X-ray photoelectron spectra satellite structures for oxide and oxygen coordination cores. Vacuum 114:162–165. https://doi.org/10.1016/j.vacuum.2014.10.013

Rahman ML, Sarkar SM, Yusoff MM (2016) Efficient removal of heavy metals from electroplating wastewater using polymer ligands front. Env Sci Eng 10:352–361. https://doi.org/10.1007/s11783-015-0783-0

Sharma L, Nishida K, Kanaya T (2005) FT-IR study of the morphological interactions in PHB/PAZO blends and their dependence on solvent variation. Polym Polym Compos 13:681–686. https://doi.org/10.1177/096739110501300704

Shi S, Li BC, Qian YX, Mei PP, Wang N (2020) A simple and universal strategy to construct robust and antibiofouling amidoxime aerogels for enhanced uranium extraction from seawater. Chem Eng J 397:125337. https://doi.org/10.1016/j.cej.2020.125337

Singh S, Bajwa BS, Kaur I (2021) (Zn/Co)-zeolitic imidazolate frameworks: room temperature synthesis and application as promising U(VI) scavengers-a comparative study. J Ind Eng Chem 93:351–360. https://doi.org/10.1016/j.jiec.2020.10.012

Tian G, Geng JX, Jin YD, Wang CL, Li SQ, Chen Z, Wang H, Zhao YS, Li SJ (2011) Sorption of uranium(VI) using oxime-grafted ordered mesoporous carbon CMK-5. J Hazard Mater 190:442–450. https://doi.org/10.1016/j.jhazmat.2011.03.066

Tolkou AK, Katsoyiannis IA, Zouboulis AI (2020) Removal of arsenic, chromium and uranium from water sources by novel nanostructured materials including graphene-based modified adsorbents: a mini review of recent developments. Appl Sci-Basel 10:3241. https://doi.org/10.3390/app10093241

Wang JL, Guo X (2020) Adsorption isotherm models: classification, physical meaning, application and solving method. Chemosphere 258:127279. https://doi.org/10.1016/j.chemosphere.2020.127279

Wang LL, Luo F, Dang LL, Li JQ, Wu XL, Liu SJ, Luo MB (2015) Ultrafast high performance extraction of uranium from seawater without pretreatment using an acylamide and carboxyl-functionalized metal-organic framework. J Mater Chem A 3:13724–13730. https://doi.org/10.1039/c5ta01972a

Wang J, Wang YM, Zhang YT, Uliana A, Zhu JY, Liu JD, Van der Bruggen B (2016) Zeolitic imidazolate framework/graphene oxide hybrid nanosheets functionalized thin film nanocomposite membrane for enhanced antimicrobial performance. ACS Appl Mater Interfaces 8:25508–25519. https://doi.org/10.1021/acsami.6b06992

Wang Y, Lin ZW, Lin HS, Liu Q, Liu J, Liu JY, Liu RR, Zhu JH, Wang J (2021a) Anti-bacterial and super-hydrophilic bamboo charcoal

with amidoxime modified for efficient and selective uranium extraction from seawater. J Colloid Interface Sci 598:455–463. https://doi.org/10.1016/j.jcis.2021.03.154

Wang YL, Long J, Xu WJ, Luo H, Liu J, Zhang YP, Li JC, Luo XG (2021b) Removal of uranium(VI) from simulated wastewater by a novel porous membrane based on crosslinked chitosan, UiO-66-NH$_2$ and polyvinyl alcohol. J Radioanal Nucl Chem 328:397–410. https://doi.org/10.1007/s10967-021-07649-4

Wang SQ, Shi L, Yu SJ, Pang HW, Qiu MQ, Song G, Fu D, Hu BW, Wang XX (2022) Effect of Shewanella oneidensis MR-1 on U(VI) sequestration by montmorillonite. J Environ Radioact 242:106798. https://doi.org/10.1016/j.jenvrad.2021.106798

Willauer HD, Hardy DR, Hardy SA, Hardy F, Williams FW, Drab DM (2015) An economic basis for littoral land-based production of low carbon fuel from nuclear electricity and seawater for naval or commercial use. Energy Policy 81:67–75. https://doi.org/10.1016/j.enpol.2015.02.006

Wu YH, Pang HW, Yao W, Wang XX, Yu SJ, Yu ZM, Wang XK (2018) Synthesis of rod-like metal-organic framework (MOF-5) nanomaterial for efficient removal of U(VI): batch experiments and spectroscopy study. Sci Bull 63:831–839. https://doi.org/10.1016/j.scib.2018.05.021

Xie LX, Zhong Y, Xiang RJ, Fu GY, Xu YZ, Cheng YX, Liu Z, Wen T, Zhao YY, Liu XQ (2017) Sono-assisted preparation of Fe(II)-Al(III) layered double hydroxides and their application for removing uranium(VI). Chem Eng J 328:574–584. https://doi.org/10.1016/j.cej.2017.07.051

Xue Y, Chen JQ, Liu P, Liu JZ, Liu YY, Liu WT, Ma FQ, Yan YD (2022) An efficient and high-capacity porous functionalized-membranes for uranium recovery from wastewater. Colloid Surf A-Physicochem Eng Asp 647:129032. https://doi.org/10.1016/j.colsurfa.2022.129032

Yamauchi T, Kaifu S, Mori Y, Kanasaki M, Oda K, Kodaira S, Konishi T, Yasuda N, Barillon R (2013) Applicability of the polyimide films as an SSNTD material. Radiat Meas 50:16–21. https://doi.org/10.1016/j.radmeas.2012.04.013

Yan Q, Wang AJ, Wang GS, Wang WJ, Chen QS (2011) Nuclear power development in China and uranium demand forecast: based on analysis of global current situation. Prog Nucl Energy 53:742–747. https://doi.org/10.1016/j.pnucene.2010.09.001

Yang WT, Bai ZQ, Shi WQ, Yuan LY, Tian T, Chai ZF, Wang H, Sun ZM (2013) MOF-76: from a luminescent probe to highly efficient U(VI) sorption material. Chem Commun 49:10415–10417. https://doi.org/10.1039/c3cc44983a

Yang WT, Pan QH, Song SY, Zhang HJ (2019) Metal-organic framework-based materials for the recovery of uranium from aqueous solutions. Inorg Chem Front 6:1924–1937. https://doi.org/10.1039/c9qi00386j

Yang XZ, Bonnett BL, Spiering GA, Cornell HD, Gibbons BJ, Moore RB, Foster EJ, Morris AJ (2021) Understanding the mechanical reinforcement of metal-organic framework-polymer composites: the effect of aspect ratio. ACS Appl Mater Interfaces 13:51894–51905. https://doi.org/10.1021/acsami.1c05430

Yi XH, Ma SQ, Du XD, Zhao C, Fu HF, Wang P, Wang CC (2019) The facile fabrication of 2D/3D Z-scheme g-C$_3$N$_4$/UiO-66 heterojunction with enhanced photocatalytic Cr(VI) reduction performance under white light. Chem Eng J 375:121944. https://doi.org/10.1016/j.cej.2019.121944

Zeng YY, Liu S, Xu JC, Zhang A, Song YX, Yang L, Pu AL, Ni YR, Chi FT (2021) ZIF-8 in-situ growth on amidoximerized polyacrylonitrile beads for uranium sequestration in wastewater and seawater. J Environ Chem Eng 9:106490. https://doi.org/10.1016/j.jece.2021.106490

Zhang AY, Uchiyama G, Asakura T (2005) PH effect on the uranium adsorption from seawater by a macroporous fibrous polymeric material containing amidoxime chelating functional group. React Funct Polym 63:143–153. https://doi.org/10.1016/j.reactfunctpolym.2005.02.015

Zhang GY, Zhuang YH, Shan D, Su GF, Cosnier S, Zhang XJ (2016) Zirconium-based porphyrinic metal-organic framework (PCN-222): enhanced photoelectrochemical response and its application for label-free phosphoprotein detection. Anal Chem 88:11207–11212. https://doi.org/10.1021/acs.analchem.6b03484

Zhang JC, Zhang HS, Liu Q, Song DL, Li RM, Liu PL, Wang J (2019a) Diaminomaleonitrile functionalized double-shelled hollow MIL-101 (Cr) for selective removal of uranium from simulated seawater. Chem Eng J 368:951–958. https://doi.org/10.1016/j.cej.2019.02.096

Zhang XM, Liu Y, Jiao Y, Gao QH, Wang P, Yang Y (2019b) Enhanced selectively removal uranyl ions from aqueous solution by Fe@ZIF-8. Microporous Mesoporous Mat 277:52–59. https://doi.org/10.1016/j.micromeso.2018.10.017

Zheng XH, Zhang Y, Wang ZQ, Wang YF, Zou LH, Zhou XS, Hong ST, Yao L, Li CL (2020) Highly effective antibacterial zeolitic imidazolate framework-67/alginate fibers. Nanotechnology 31:375707. https://doi.org/10.1088/1361-6528/ab978a

Zhu J, Qiu WW, Yao CJ, Wang C, Wu DQ, Pradeep S, Yu JY, Dai ZJ (2021a) Water-stable zirconium-based metal-organic frameworks armed polyvinyl alcohol nanofibrous membrane with enhanced antibacterial therapy for wound healing. J Colloid Interface Sci 603:243–251. https://doi.org/10.1016/j.jcis.2021

Zhu MX, Liu LJ, Feng J, Dong HX, Zhang CH, Ma FQ, Wang Q (2021b) Efficient uranium adsorption by amidoximized porous polyacrylonitrile with hierarchical pore structure prepared by freeze-extraction. J Mol Liq 328:115304. https://doi.org/10.1016/j.molliq.2021.115304

Zhu L, Zhang CH, Ma FQ, Bi CL, Zhu RQ, Qin FF, Liu LJ, Bai JW, Dong HX, Satoh T (2022) Oxime-modified hierarchical self-assembly polyimide microspheres for high-efficient uranium recovery from wastewater. Environ Sci-Nano 9:1168–1179. https://doi.org/10.1039/d1en01046h

Authors and Affiliations

Changlong Bi[1] · Chunhong Zhang[1,2] · Chao Wang[1,2] · Lien Zhu[1] · Ruiqi Zhu[1] · Lijia Liu[1,2] · Yudan Wang[1] · Fuqiu Ma[2,3] · Hongxing Dong[1]

✉ Chunhong Zhang
   zhangchunhong97@163.com

[1] Key Laboratory of Superlight Materials and Surface Technology of Ministry of Education, College of Materials Science and Chemical Engineering, Harbin Engineering University, Harbin 150001, People's Republic of China

[2] Yantai Research Institute of Harbin Engineering University, Yantai 264006, People's Republic of China

[3] College of Nuclear Science and Technology, Harbin Engineering University, Harbin 150001, People's Republic of China